Numerical simulation of laminar-turbulent transition on a dolphin using the γ-Re$_\theta$ model

D. Riedeberger and U. Rist

Institut für Aerodynamik und Gasdynamik, Universität Stuttgart, Pfaffenwaldring 21, D-70550 Stuttgart, Germany, email: lastname@iag.uni-stuttgart.de

Summary. The γ-Re$_\theta$-model, a two equation, correlation-based transition model using local variables, has been employed to predict the extension of the laminar regions on a stiff geometry of the common dolphin (delphinus delphis) moving in the Reynolds regime of $5.5 \cdot 10^5$ to 10^7. Mesh independence was gained for a domain resolution of approximately 30 million cells in an unstructured polyhedral mesh with a prismatic wall region ($y^+ \approx 1$). The final results conclude with very limited laminar regions and thus a mainly turbulent flow around the body of a dolphin travelling at the usual speed of 3 m/s and a resulting drag coefficient of $C_D \approx 0.004$ referring to the wetted surface area of $A = 1.571$ m^2. Consequently the potential for active laminarisation due to the anisotropic structure of the dolphin skin is well established and is estimated to be as high as 20 % with respect to drag force reduction.

1 Introduction

The inherent differences in laminar and turbulent flow characteristics relating to skin-friction are not only a great issue in industrial application but also fed the discussion on dolphin locomotion for a long time in the past century. Whether the dolphin shows a potential to extend the laminar flow region and thus reduce the drag force on its body has been in question since the proposition of Gray's paradox [4] and has recently been revisited in a broader review [3]. Newly developed modelling approaches based on experimental correlations for transition onset together with eddy-viscosity turbulence models for the Reynolds-Averaged Navier-Stokes equations (RANS) of unstructured flow solvers enable the study of transitional flow around complex geometries. Together with the present support of High Performance Computers (HPC) it is now possible to simulate the flow around the dolphin sufficiently accurate with a discretization of a rigid model with inclusion of the boundary layer characteristics and the application of turbulence and transition modelling. As a result, the Reynolds-number-dependent transition behaviour as well as the

influence of the turbulence level in the free-stream on the onset of turbulent flow can be addressed and an estimation of the potential for active laminarisation of the dolphin skin can be given.

The governing equations and the transition model formulation is outlined in section 2. Afterwards the numerical details are given. The results of the flow around the dolphin are presented and discussed in part 4 followed by an overview of the computational performance in section 5. A conclusion summarizes the achievements.

2 Physical Modelling

The fluid flow is modelled based on the incompressible Navier-Stokes equations for a fluid with constant properties.

$$\nabla \cdot \boldsymbol{u} = 0 \tag{1}$$

$$\rho \frac{D\boldsymbol{u}}{Dt} = \rho \boldsymbol{f} - \nabla p + \nabla \cdot \boldsymbol{\tau} \tag{2}$$

The energy equation has been omitted here as the calculations dealt with incompressible flow and thus the energy equation can be treated as decoupled from momentum and mass conservation. For convenience the above equations can be adequately non-dimensionalized delivering the formulation with regard to the Reynolds number in the momentum equation as they can be found continuously in the literature [14].

RANS equations and turbulence closure

To regard flows that are inherently turbulent it is feasible to use the Reynolds-decomposition leading to the Reynolds-Averaged Navier-Stokes equations in the form of

$$\frac{\partial \overline{u}}{\partial x} + \frac{\partial \overline{v}}{\partial y} + \frac{\partial \overline{w}}{\partial z} = 0 \tag{3}$$

$$\rho \frac{\partial \bar{u}_i}{\partial t} + \rho \left(\frac{\partial \bar{u}_i \bar{u}_j}{\partial x_j} \right) = \bar{f}_i - \frac{\partial \bar{p}}{\partial x_i} + \eta \frac{\partial}{\partial x_j} \left(\frac{\partial \bar{u}_i}{\partial x_j} + \frac{\partial \bar{u}_j}{\partial x_i} - \frac{2}{3} \frac{\partial \bar{u}_k}{\partial x_k} \delta_{ij} \right) - \rho \left(\frac{\partial}{\partial x_j} \overline{u_i' u_j'} \right) \tag{4}$$

where Cartesian notation was used.

For turbulence closure the Boussinesq approximation is used in the eddy viscosity formulation of the SST-k-ω model [9] that is adapted related to the transition model formulation [10].

Correlation-Based Transition Modelling

The γ-Re_θ-transition modelling relies on empirical correlations that relate the onset of transition to the boundary layer's momentum-thickness Reynolds number. This approach bases on the early works of Abu-Ghannam and Shaw [1] which obtained a functional relationship for the transition onset with respect to free-stream-turbulence level and pressure gradient in the form $\mathrm{Re}_{\theta t} = f(\mathrm{Tu}, \lambda_\theta)$ - where λ_θ is the Thwaites pressure gradient parameter. This empirical basis has been further refined and extended to low free-stream-turbulence environments by Menter and Langtry [6]. As the evaluated boundary layer momentum thickness is an integral parameter, the work of Menter et al. [10] proposed to use the relation between Re_θ and the local vorticity-Reynolds number $\mathrm{Re}_V = \Omega \rho y^2/\mu$ which is a locally available scalar value. The formulation $\mathrm{Re}_\theta = \max(\mathrm{Re}_V)/2.193$ enables reconstruction of the non-local value from a locally available one. The fact that this matching becomes improper for stronger deviations of the shape factor from the Blasius solution is actually used in the model for capturing the separation behaviour [10].

The onset criterion for transition - empirically known in the free-stream by the previous definitions - is further transported as $\widetilde{\mathrm{Re}}_{\theta t}$ inside the boundary layer using the following function

$$\frac{\partial(\rho\widetilde{\mathrm{Re}}_{\theta t})}{\partial t} + \frac{\partial(\rho u_j \widetilde{\mathrm{Re}}_{\theta t})}{\partial x_j} = P_{\theta t} + \frac{\partial}{\partial x_j}\left[\sigma_{\theta t}\left(\mu + \mu_t\right)\frac{\partial \widetilde{\mathrm{Re}}_{\theta t}}{\partial x_j}\right]. \tag{5}$$

Based on this flow field variable an intermittency scalar γ causes the production terms of the underlying SST turbulence model to be switched on according to the equation

$$\frac{\partial(\rho\gamma)}{\partial t} + \frac{\partial(\rho u_j \gamma)}{\partial x_j} = P_\gamma - E_\gamma + \frac{\partial}{\partial x_j}\left[\left(\mu + \frac{\mu_t}{\sigma_f}\right)\frac{\partial \gamma}{\partial x_j}\right]. \tag{6}$$

In both cases P and E reassemble production and destruction terms respectively which are given by the model formulation of Menter [10], [11] and who further demand the specification of correlations [6] based on experiments to close the formulation. The necessary model inherent correlations, first kept proprietary, were proposed by different researchers [13], [7] before finally published by Langtry and Menter [6]. Concerning the implementation into the solver STAR-CCM+ some minor adaptations were proposed and the documentation by Malan et al. [8] is best consulted to get an overview on these.

3 Numerical Details

For the volume mesh generation within the software STAR-CCM+ by cd-adapco unstructured, polyhedral cells were used combined with prismatic,

wall-adjacent cells sufficiently fine to achieve values of a dimensionless distances of $y^+ \approx 1$ and well below that. Prior studies within the scope of this work assessed the model implementation using a flat-plate and an axisymmetric air-ship body. Various mesh topologies (hexahedral, polyhedral), cell densities (100 to 400 surface nodes per characteristic length) as well as different wall-normal refinements were considered. As a result the best-practise for the generation of the volume mesh for the transition simulations on the dolphin were found to use at least 100 nodes across the body length together with automatic local mesh refinements in areas of high curvature. The first wall-adjacent prismatic cell was 10^{-5} m high and expanded with a ratio of 1.1 to an overall boundary mesh thickness of 3.5 to 5 mm. As the dolphin model has an overall characteristic length of $L = 1.94$ m this relates to a near-wall mesh of the order of 0.26 % compared to the body dimension. It was found that the choice of the wall-normal mesh resolution is most important for the transition modelling as already published before [5]. Thus a slight upstream shift of transition is found for y^+ values above unity and the range between $y^+ = 0.01$ and $y^+ = 1$ delivers results best matched to experimental studies [5] . A mesh study on a dolphin model without fins enabled a proper addressing of any mesh-related qualitative offsets and thus the cases presented within this report are judged to be mesh independent. The volume mesh was coarsened to the boundaries using hanging-node refinement and the domain borders were at least 2.5 times the body length ($L = 1.94$ m) away from the dolphin surface - placement of the boundaries of ten times this value were showing no qualitative and no major quantitative differences in the results. The domain was bounded by a subsonic velocity inlet, a pressure outlet (with preceding 5 m of extruded mesh), slip walls on the outer boundaries and no-slip surfaces on the dolphin. Preconditioning of the field was not straight-forward due to the complex geometry. Thus the flow was allowed to develop from an initially resting fluid.

For the flow simulations the rigid body with pectoral and dorsal fins and tail fluke consisted of a volume mesh of around 30.5 million polyhedral cells. Studies on mesh-density and a great set of free-stream-turbulence intensity as well as Reynolds-number variations were done on a 16 million cell model of the dolphin without any fin appendices.

Within the solver STAR-CCM+ the governing and modelling equations are addressed in a finite-volume method used with cell-centered discretization. A segregated, implicit approach with Rhie-Chow interpolation [2] based on the AMG SIMPLE algorithm is applied to the flow and energy equations. The transport equations for momentum, for the modelling of SST-k-ω as well as the γ-Re_θ-model are implemented using second-order upwinding.

4 Results and Discussion

The flow of water around the full dolphin body was taken for varying Reynolds numbers ranging from $Re_L = 0.54 \cdot 10^6$ to $Re_L = 5.4 \cdot 10^6$ which relate to velocities of the free-stream from $u_\infty = 0.25$ to $u_\infty = 2.5$ m/s. The plots of the turbulent kinetic energy of the wall-adjacent cell is given in figure 1. In these plots the high values at the leading edges of the fins locally exceed the maximum of the highest contour plot value out of reasons to facilitate a better plotting of the main transition phenomena.

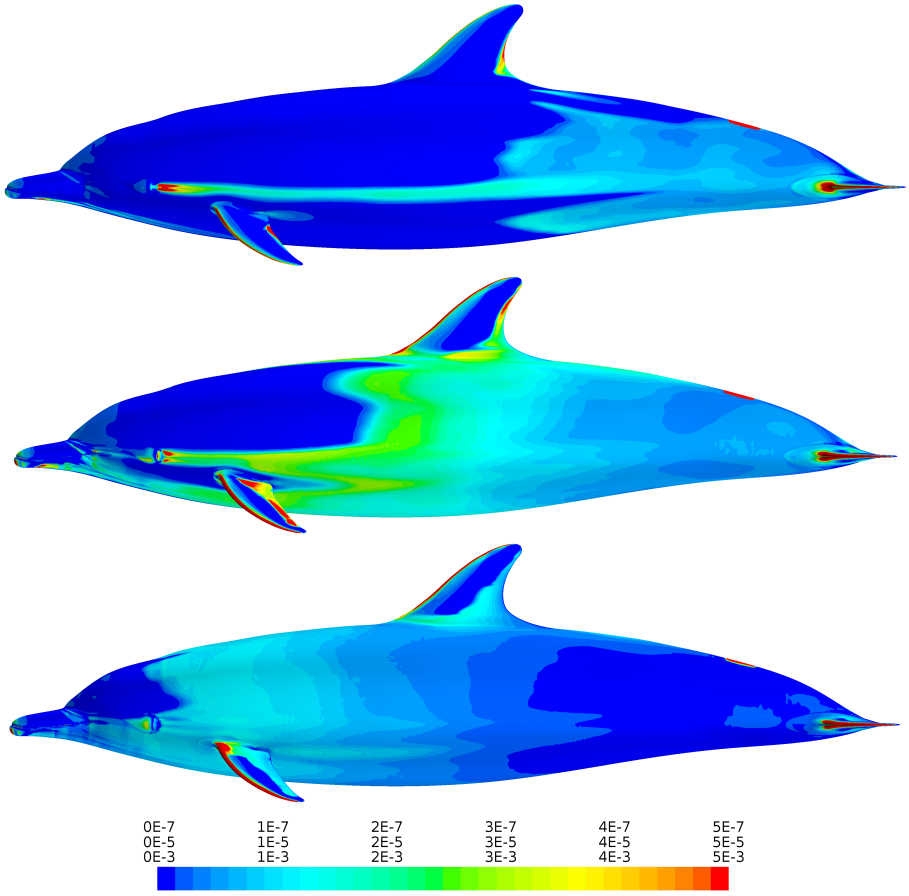

Fig. 1. Turbulent kinetic energy k for free-stream velocities of $u_\infty = 0.25$ (upper), 1.0 (mid) and 2.5 m/s (lower), turbulence intensity $Tu = 1\%$

Clearly there is a visible transition process taking place whose location is shifting upstream with increasing free-stream flow Reynolds number. While

at low velocities the eye serves as a turbulence trip and only few portions of the body are experiencing turbulent characteristics the higher free-stream velocities cause the flow to be mainly turbulent only leaving very short laminar patches on the forehead of the dolphin. Additional insight into the flow development and the dependence on the Reynolds number can be found when the turbulent kinetic energy is plotted in tomograms perpendicular to the stream-wise extent of the body as given in figure 2. At a velocity of 1 m/s

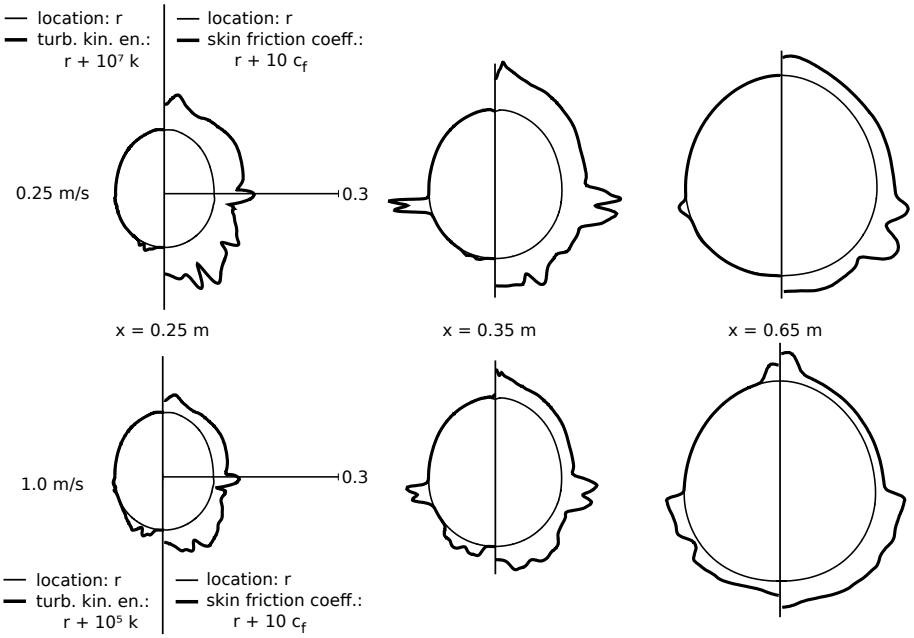

Fig. 2. Tomograms of k and C_f at different downstream body locations $x = 0.25, 0.35, 0.65$ m for $u_\infty = 0.25$ m/s (upper) and $u_\infty = 1.0$ m/s (lower), $Tu = 1\%$, observation of body transition

both the eye and the breath hole can be identified to cause the local transition to turbulence to set in. As visible, the plot at $x = 0.35$ m just behind the location of the eye (centered approx. $x = 0.3$ m) shows a raise in turbulent kinetic energy k correlating with an increase in skin friction. Similarly, after the breath hole at location $x = 0.65$ both skin friction and turbulent energy are elevated compared to the lateral parts of the body. In addition it is evident from the given tomograms for 1 m/s that the snout is shedding a broad turbulent fraction at the lower body which extends further below the pectoral fins. It is the believe of the authors that the cause of this lies in vortical structures that develop around the shape of the snout and that these are forced to follow along the lower parts of the body due to downward-facing streamlines on the connection to the forehead. Indeed one can identify such

a raise in turbulent kinetic energy on the lower body for the 0.25 m/s flow as well at a location $x = 0.25$ m and less intense at $x = 0.35$ m. It is seen that the onset of turbulence is suppressed in the direction of the flow, most probably due to favourable pressure gradients caused by the geometric body shape. The importance of the pressure gradient on transition suppression can be verified if one looks at figure 3 where the dimensionless pressure coefficient built with the free stream velocity $u_\infty = 1.0$ m/s is plotted on the surface of the dolphin. This pressure distribution was also found to be representative for all the incompressible calculations within this Reynolds-number regime. Quite obviously, the frontal regions of snout and head are exposed to the

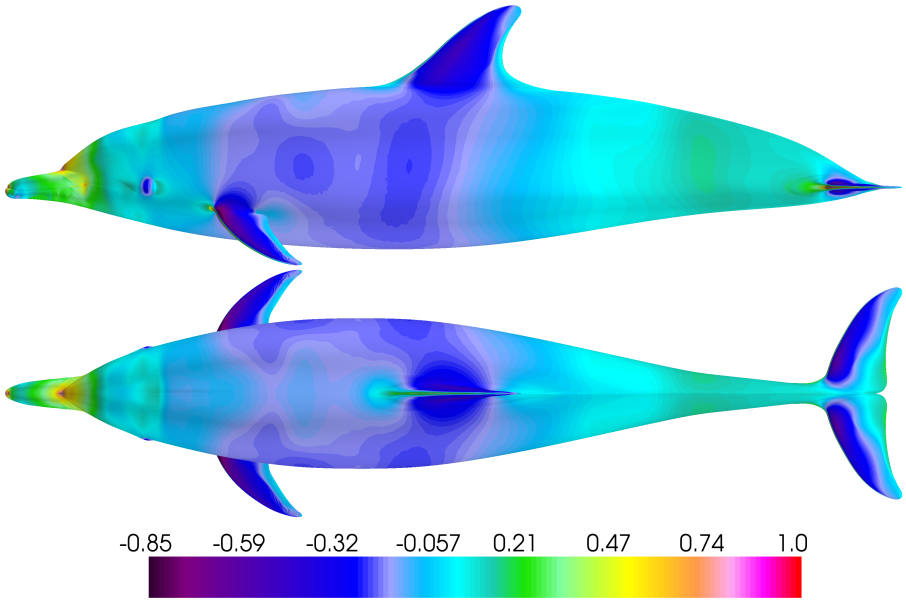

Fig. 3. Distribution of pressure coefficient C_p for free-stream velocities of $u_\infty = 1.0$ m/s, side (upper) and top (lower) projection, turbulence intensity $Tu = 1\%$

flow and build stagnation regions while the downstream portion of the body experiences acceleration resulting in decreasing static pressure until mid-way through the body where a large region of minimal pressure extends from the pectoral to the dorsal fin. Thus, the region of the body downstream of the connection of the fin appendices is governed by adverse pressure gradients. A more closer look on the pressure distribution for the appendices will follow later in the report.

If the flow patterns are observed more closely, the streamlines along the body can be consulted. They are given in figure 4 for a rake position just upstream of the snout. At first it is obvious that the appendices of both the

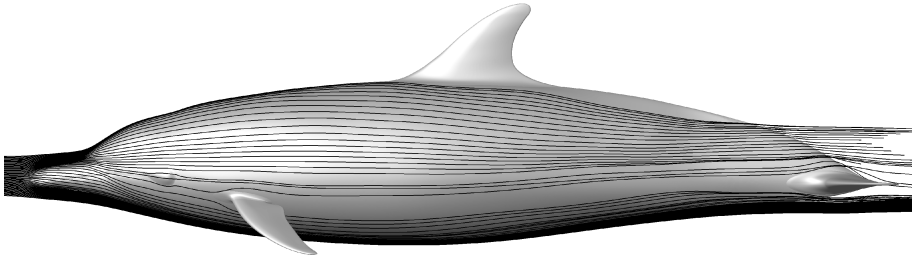

Fig. 4. Streamlines along the dolphin body for $u_\infty = 1.0$ m/s, $Tu = 1\%$

pectoral and the dorsal fin influence the flow pattern along the body in a way that they cause the streamlines to aim away from the fins resulting in wake regions behind them. In addition the influence of the snout is visible. As already anticipated from the distribution of turbulent kinetic energy on the body there is a region present at the lower front body where the flow is forced downwards due to the shape of the snout and the connection region to the head.

Another analysis of the flow patterns around the body focuses on the fin appendices. Although the streamlines along the appendices are not given within this text to keep a brief overview the results of velocity distribution and stream line patterns seemed to support the studies already done by Pavlov on the dorsal fin [12]. The profile shape and pressure distribution on the appendices was gained by creating cut sections along the chord approximately midway through the extent of each fin. This related in a chord length of $L = 0.0929$ m for the pectoral fin, $L = 0.1413$ m for the dorsal fin and $L = 0.1155$ m for the tail fluke of the dolphin. The respective profile shapes and the resulting pressure distribution is given in figure 5. Both the pectoral and dorsal fin show to have a slightly delayed maximum thickness which potentially makes them laminar profiles. The pressure distributions are accordingly while the pectoral fin has to be specially regarded as angled to the flow direction other than the dorsal fin and the tail fluke. Thus, the location of the lowest pressure is not relating to the thickest point as is the case for the dorsal fin and tail fluke. If one wants to draw conclusions concerning transitional behaviour of the fin appendices figure 1 can be consulted. More conveniently the skin-friction coefficient across the chord length of the fins is given in figure 6. In all cases the skin friction shows laminar behaviour almost half way through the chord length of the fins. In most of the lower- or middle-Reynolds-number cases transition seems to be triggered by separation on the pectoral fin and the tail fluke. In addition it has to be noted that the maximum skin-friction coefficient for the pectoral fin is located further downstream than compared to the other appendices due to the angled arrangement in the flow. The transition behaviour of the fins is not surprising as one has to take into account that the characteristic length of the fin appendices is one order of magnitude smaller

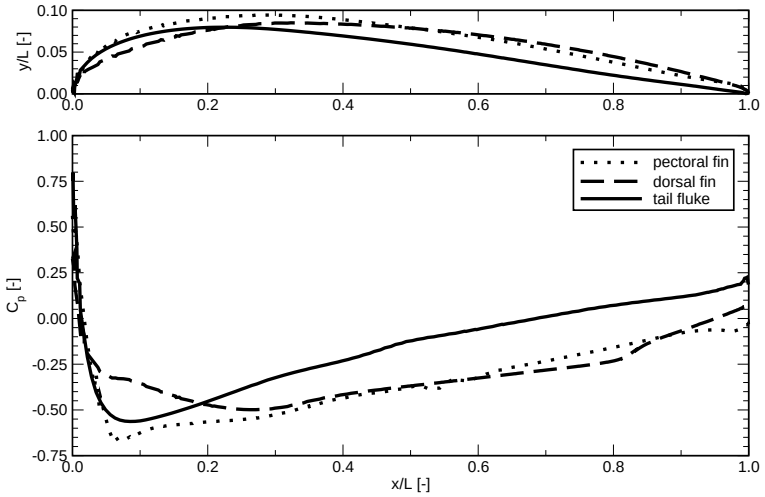

Fig. 5. Shape and C_p distribution for the fin appendices

than the body and thus the Reynolds-number regime accordingly is lower relating to smaller disturbances in the flow fluctuations.

Concerning the body forces that act on the dolphin as a result of the transitional flow it was found that with rising turbulence level also the overall drag coefficient C_D is seen to rise whereas a Reynolds-number dependence was not possible to be extracted clearly. Thus, for the given regime of free-stream flow from 0.25 to 5 m/s an average value of $\overline{C_D} = 0.0038$ (standard deviation 0.00026) was found using a representative model of the dolphin without inclusion of the fins. As a means to evaluate possible laminarization potentials a figurative calculation was pursued. For the cases of $u_\infty = 1$ and $u_\infty = 2.5$ m/s the drag coefficient for a low turbulence case ($Tu = 0.0025$) at which transition only occurs very late on the body was utilized for calculating the drag force on a high turbulence case ($Tu = 0.01$) with early transition at the same velocity. As a result the force acting on the body was reduced by 18.3 % to 26.7 % for the high and low velocity respectively. This is meant to give a ball-park figure of existing potential for active laminarization. It remains to apply turbulence damping models or other ways to simulate laminar patches in transitional flow simulation to support this view in future numerical studies.

5 Computational Resources and Performance of the Solver STAR-CCM+

The present study was done using the NEC Nehalem Cluster at HLRS with two quad core CPU, 12 GB RAM per node and infiniband network connection. The version 5.04.006 of the commercially available solver STAR-CCM+

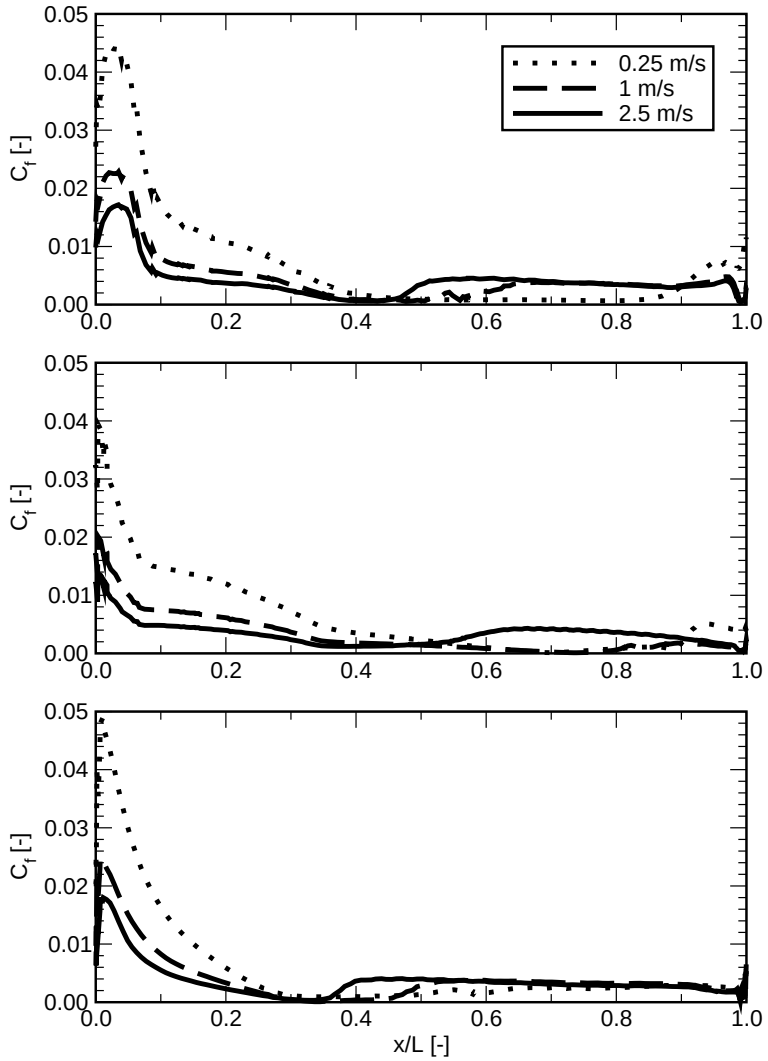

Fig. 6. Skin friction coefficient C_f along the pectoral (top) and dorsal (middle) fin and the tail fluke (bottom), Tu = 1%, $\mathrm{Re}_L = 0.544 \cdot 10^6 \ldots 1.089 \cdot 10^7$

from cd-adapco was used which has a client-server architecture and automatically partitions the mesh, distributes the partitions to the machine processes and controls data exchange via an additionally placed control-process. Due to the necessary grid refinement in the wall-adjacent boundary layer and the complexity of the dolphin shape the grid generation was pursued on one node with increased memory of at least 48 GB. For most of the parametric studies 48 processes on 8 nodes with 12 GB each were used relating to 650,000 cells

placed per core to gain a sufficient balance between workshare and communication. While overall convergence for the momentum and continuity equations was already gained after 4000 iterations in 42 hours elapsed time the turbulence and transition model equations were observed until 8000 iterations at an overall time of approximately 84 hours.

Evaluating the performance of a transitional simulation in comparison to a solely turbulent RANS simulation table 1 gives an overview. There the calculations ran on 8 nodes with 63 processes in total and the convergence in those cases was achieved as continuity and y-momentum residuals reached 10^{-5} and turbulent kinetic energy settled at a residual of $4 \cdot 10^{-4}$. While the first simulation only used an activated SST-k-ω model the second run also iterated on the two transport equations of the γ-Re_θ transition model. Obviously the

Table 1. Performance of turbulent and transitional calculation on full dolphin body on NEC-Nehalem

used models	CPU (nodes)	iterations	run time [h]	I/O [min]
SST-k-ω	63 (8)	3791	15.09	15.6
SST-k-ω + γ-Re_θ	63 (8)	2543	28.05	23.2

need for solving two additional transport equations adds to the computational time. While the turbulent calculation iterates longer to reach convergence it still results in a shorter overall run time compared to the case with activated transition modelling. This increase to almost twice of the solution time can be reasoned by two things. First, the solution of the additional equations demands longer iteration time. Second, also the implementation of the transition model into the solver demands the global broadcast of the location of the cells close to the boundary layer edge as a tree to all mesh partitions every several iterations which consequently produces overhead when run in parallel [8]. The mentioned I/O time reported within table 1 results from the writing of restart files and is higher for the transitional case as the file sizes are higher in this case as well.

To judge the scalability of the solver figure 7 shows total solver-elapsed-times for simulations running on 1 to 31 processors on dedicated one to four nodes. The respective calculations were all run until residuals for continuity below 10^{-5} were achieved. Obviously the application scales quite well and distributing the mesh partitions leads to a good reduction in overall solution time. It is necessary to place an additional control process for each running simulation within the STAR-CCM+ solver which handles communication between the workers and the host. Consequently, the processes of 7, 15 and 31 relate to fully used nodes with one additional control process each. In similar runs of the simulation it was observed, that placing this control task on a node outside of completely covered working nodes (e.g. 32 processes on four nodes plus one control process on an additional node) relates to quite some added

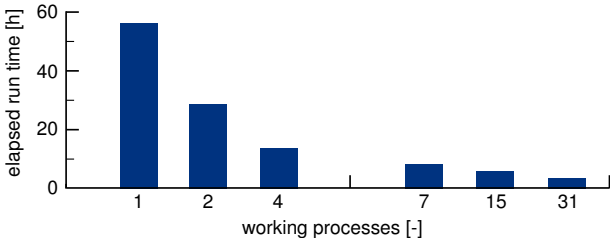

Fig. 7. Elapsed run time of transitional simulation for different number of working processes on the NEC Nehalem cluster

time in communication and thus in a deviation from the expected scaling. This effect is most obvious if one takes a look at calculations within one node (max. 8 processors). While the scaling from one to seven processors (plus controller) is almost exponential the placement of the controller outside the fully used node raises the overall solution time to 12.23 h as opposed to 8.23 h for a run on seven nodes. As more nodes are used this effect becomes less important which is reasonable as communication overhead is enhanced for global node communication anyway. Furthermore it was observed that the automatic partitioning of the mesh also resulted in spurious oscillations in a few cases which lead to a far extended run time to reach convergence. Overall it has to be noted that all scaling evaluations of the solver were done during normal operation of the Nehalem cluster of the HLRS and no special precautions could be taken to especially reserve whole nodes or blades exclusively.

Nevertheless it is obvious that STAR-CCM+ easily enables to profit from HPC infrastructures with MPI interface but that mesh partitioning and parallelisation optimization for a specific machine environment is much more cumbersome than with codes that can be user-adapted and tailored to the computational environment.

6 Conclusions

The possibilities to account for a broad range of physical influences on the transition phenomenon has been well implemented into unstructured CFD codes through the γ-Re_θ model by Menter and Langtry [6], and the application to STAR-CCM+ by Malan et al. [7]. Due to the modelling of both turbulence and transition within the framework of the RANS equations it is now possible to use HPC to address complex geometric setups as opposed to direct numerical simulation which, at using the same computational costs, focus on the underlying physics in simple flow geometries. The advantage of correlation-based modelling for turbulence onset also enables the transition model to gain precision if the onset criteria are fed with more sophisticated parametric studies through either experiments or DNS.

Using this transition model coupled to the eddy-viscosity turbulence-closure by the SST-k-ω model flow around half-symmetric three-dimensional dolphin geometries with fin appendices could be pursued. Regarding normal swimming speeds of the dolphin around 3 m/s in a 1% turbulence-intensity environment it was found that the flow around the dolphin is mainly turbulent with limited laminar regions at the front of the head. Parametric studies concerning different environments of turbulence intensity were used to show the strong influence of turbulence level on the shear-force contribution of the overall drag. The flow pattern around the rigid, full body resulted in a drag coefficient of $C_D \approx 0.004$ which is in the same order of magnitude as found in literature. With this knowledge it was possible to roughly estimate drag reductions of around 20 % if laminarisation techniques exist that can delay the onset of turbulence to locations comparable to lower values of turbulence intensity. Furthermore the strong impact of turbulence level in the free-stream for transition occurrence and location emphasizes the demand to investigate the typically present turbulence values in the marine surrounding to be able to simulate the swimming environment and flow characteristics of the dolphin in closer match to reality.

In conclusion the flow around a rigid dolphin model in the regime of $\mathrm{Re}_L > 5 \cdot 10^6$ shows transition in very early locations. The limited laminar regions endure the hope of active laminarisation potential due to e.g. certain structure (i.e. compliant walls or surface roughness) of the dolphin skin.

Aknowledgements
The authors greatly appreciate the support by Vadim V. Pavlov who kindly provided the CAD data of the dolphin model that was the basis of the simulations. In addition the grant of computation time on the NEC Nehalem cluster of the High Performance Computing Center Stuttgart (HLRS) in the framework of the LAMTUR project is highly thanked for as well.

References

[1] B. J. Abu-Ghannam and R. Shaw. Natural transition of boundary layers - the effects of turbulence, pressure gradient and flow history. *Journal Mechanical Engineering Science*, 22(5):213–228, 1980.

[2] I. Demirdzic and S. Muzaferija. Numerical method for coupled fluid flow, heat transfer and stress analysis using unstructured moving meshes with cells of arbitrary topology. *Computer Methods in Applied Mechanics and Engineering*, 125(1-4):235–255, 1995.

[3] F. E. Fish. The myth and reality of gray's paradox: implication of dolphin drag reduction for technology. *Bioinspiration & Biomimetics*, 1(2):R17–R25, 2006.

[4] J. Gray. Studies in animal locomotion: Vi. the propulsive powers of the dolphin. *Journal of Experimental Biology*, 13:192–199, 1936.

[5] R. B. Langtry. *A Correlation-Based Transition Model using Local Variables for Unstructured Parallelized CFD codes*. PhD thesis, Universität Stuttgart, 2006.

[6] R. B. Langtry and F. R. Menter. Correlation-based transition modeling for unstructured parallelized computational fluid dynamics codes. *AIAA JOURNAL*, 47(12):2894–2906, December 2009.

[7] P. Malan, K. Suluksna, and E. Juntasaro. Calibrating the γ-Re_θ transition model. In *ERCOFTAC Bulletin 80*, pages 53–57.

[8] P. Malan, K. Suluksna, and E. Juntasaro. Calibrating the γ - Re_θ transition model for commercial cfd. In *47th AIAA Aerospace Sciences Meeting*, January 2009.

[9] F. R. Menter. Two-equation eddy-viscosity turbulence models for engineering applications. *AIAA*, 32(8):1598–1605, August 1994.

[10] F. R. Menter, R. B. Langtry, S. R. Likki, Y. B. Suzen, P. G. Huang, and S. Völker. A correlation-based transition model using local variables - part i: Model foundation. *Journal of Turbomachinery*, 128:413–422, July 2006.

[11] F. R. Menter, R. B. Langtry, S. R. Likki, Y. B. Suzen, P. G. Huang, and S. Völker. A correlation-based transition model using local variables - part ii: Test cases and industrial applications. *Journal of Turbomachinery*, 128:423–434, July 2006.

[12] V. V. Pavlov. Dolphin skin as a natural anisotropic compliant wall. *Institute of Physics Publishing: Bioinspiration & Biomimetics*, 1:31–40, 2006.

[13] K. Suluksna, P. Dechaumphai, and E. Juntasaro. Correlations for modeling transitional boundary layers under influences of freestream turbulence and pressure gradient. *International Journal of Heat and Fluid Flow*, 30: 66–75, 2009.

[14] F. M. White. *Viscous Fluid Flow*. McGraw-Hill Series in Mechanical Engineering, 2 edition, 1991.